J. Appl. Comput. Mech., 5(3) (2019) 540-551
DOI: 10.22055/JACM.2018.24125.1172

ISSN: 2383-4536
jacm.scu.ac.ir

M&MoCS

Shahid Chamran University of Ahvaz

Journal of Applied and Computational Mechanics

Research Paper

Evaluation of Fracture Parameters by Coupling the Edge-Based Smoothed Finite Element Method and the Scaled Boundary Finite Element Method

M. Surendran[1], A. L. N. Pramod[2], S. Natarajan[2]

[1] CSIR-Structural Engineering Research Centre, Chennai-600113, India

[2] Integrated Modelling and Simulation Lab, Department of Mechanical Engineering, Indian Institute of Technology Madras, Chennai-600036, India.

Received November 17 2017; Revised December 31 2017; Accepted for publication January 19 2018.
Corresponding author: S. Natarajan, snatarajan@cardiffalumni.org.uk

Abstract. This paper presents a technique to evaluate the fracture parameters by combining the edge based smoothed finite element method (ESFEM) and the scaled boundary finite element method (SBFEM). A semi-analytical solution is sought in the region close to the vicinity of the crack tip using the SBFEM, whilst, the ESFEM is used for the rest of the domain. As both methods satisfy the partition of unity and the compatibility condition, the stiffness matrices obtained from both methods can be assembled as in the conventional finite element method. The stress intensity factors (SIFs) are computed directly from their definition. Numerical examples of linear elastic bodies with cracks are solved without requiring additional post-processing techniques. The SIFs computed using the proposed technique are in a good agreement with the reference solutions. A crack propagation study is also carried out with minimal local remeshing to show the robustness of the proposed technique. The maximum circumferential stress criterion is used to predict the direction of propagation.

Keywords: Stress intensity factor; Singularity; Edge based smoothed finite element method; Scaled boundary finite element method.

1. Introduction

In fracture mechanics, the analysis of cracked bodies includes evaluating the stress intensity factors (SIFs) which characterize the near crack-tip stress fields. Though analytical solutions are available to evaluate the SIFs for several cases, when it comes to unconventional geometries, numerical methods are the only choice. Several methods have been developed such as the finite element method (FEM), the boundary element method (BEM), the extended finite element method (XFEM), the phantom node method [1 , 2], meshfree methods, the scaled boundary finite element method (SBFEM), the smoothed finite element method (SFEM), the natural element method (NEM) [3], and the iso-geometric analysis (IGA) [4]. However, there are still ongoing challenges and there is a continuous demand and effort from the industry and academics towards obtaining an optimal solution in terms of computational time and accuracy.

Fracture, being a very complex phenomenon, requires special methods to obtain accurate results. Since every method has its own advantage and disadvantage, combining methods so that one can complement the other is an elegant approach [5, 6]. The FEM, being highly versatile in the lot, has been coupled with several methods. For example, the Smoothed XFEM (SmXFEM) was developed by combining the smoothed FEM (SFEM) [7] with the XFEM in [8] to ease the numerical integration. Recently, the second order smoothing has also been successfully used in combination with the XFEM yielding better results [9]. The SFEM is a versatile method which was introduced to the FEM framework by Liu et al. after being successfully used with meshfree methods. The method eliminates the requirements of the derivatives. It has been widely used for polygonal elements too recently [10, 11, 12] due to its versatility. Since we are using simplex meshes, we propose to use strain smoothing which is found to be advantageous compared with the regular FEM. In particular, we use the edge based smoothed finite element method (ESFEM) [13]. The ESFEM has been shown to be superior, in terms of both accuracy and convergence, to the conventional FEM and also it possesses the advantages of the SFEM such as being applicable to any n-sided polygonal element, doing away with the computation of derivatives, and also reducing mesh dependency. However, in order to better capture the solution in the singular region we propose to use the SBFEM.

Though SBFEM was first introduced to evaluate the dynamic stiffness matrix for an infinite domain [14], it was later extended to solve problems in finite domain [15]. Recently, it has been widely used for polygonal elements [16]. Since the method doesn't require a fundamental solution, it has been very useful for solving problems which involve singularities such as in fracture mechanics [17]. In [18] the method was combined with the XFEM in order to circumvent the need for singular basis functions. It was also widely used to evaluate the fracture parameters of different materials like piezo-electric materials [19], functionally graded materials [20], elastoplastic materials [21], and anisotropic biomaterials [22].

Therefore, in this approach, we propose to use the SBFEM and ESFEM in tandem to solve linear elasto-static problems involving singularities. The SBFEM is used in the vicinity of the crack tip and the ESFEM is used in the rest of the domain. The theoretical formulation of the ESFEM is presented in Section 2. We also present the governing equations and elaborate on the stiffness matrix computation. The formulation of the SBFEM is presented in Section 3 including the SIFs evaluation. The procedure for coupling both the methods is explained in Section 4. Finally, some numerical examples solved in linear elastic fracture mechanics regime are shown in Section 5 to demonstrate the accuracy and the convergence of the proposed technique, followed by concluding remarks.

2. Formulation of edge based smoothed finite element method

The strain smoothing [23] was first used in the meshfree methods to avoid instabilities that arose in nodal integration due to vanishing derivatives at the nodes. This was solved by using an averaged strain over each integration domain. Later, the strain smoothing technique was applied to the FEM by Liu et al [7] and named SFEM. The SFEM combined the advantages of the FEM such as the use of simplex meshes and the smoothing technique which requires only the shape functions to compute the strains rather than the derivatives as in the conventional FEM. The SFEM basically involves subdivision of the element into a number of sub-cells over which the strain is spatially averaged. This averaging depends on the integration domain. This could be formed based on elements [7], nodes [24], or edges [13].

2.1 Governing equations

In SFEM, the smoothed strains are obtained as the spatial average of the compatible strain field in the smoothing domain which need not be the element in general. The procedure for arriving at the stiffness matrix is the same as FEM, only in case that smoothed strains are used instead. Consider a linear elastic 2D domain Ω with boundary Γ. The external tractive forces are applied along Γ_t and known displacement conditions are applied along Γ_u. In the absence of body forces, the governing equations are given by

$$\nabla \cdot \boldsymbol{\sigma} = \mathbf{0} \quad \text{in} \quad \Omega \tag{1}$$

The boundary conditions are described as follows:

$$\boldsymbol{\sigma} \cdot \mathbf{n} = \bar{\mathbf{t}} \quad \text{on} \quad \Gamma_t \tag{2a}$$

$$\mathbf{u} = \bar{\mathbf{u}} \quad \text{on} \quad \Gamma_u \tag{2b}$$

where, ∇ is the divergence operator, $\boldsymbol{\sigma}$ is the Cauchy stress tensor, $\mathbf{n}$ is the unit outward normal, and $\bar{\mathbf{t}}$ is the applied tractive stress. Under the assumption of small displacements and strains, the strain can be written as

$$\boldsymbol{\varepsilon} = \nabla_s \mathbf{u} \tag{3}$$

where ∇_s is the symmetric part of the gradient operator. The constitutive relation is given by

$$\boldsymbol{\sigma} = \mathbf{C} : \boldsymbol{\varepsilon} \tag{4}$$

The constitutive relations, the strain displacement, and the boundary conditions are substituted into Eq. (1). The resulting equation is multiplied by a test function and integrated in the domain by making use of the Gauss Divergence theorem after which the strong form of the PDE (Eq. (1)) is converted into an equivalent weak form as in Eq. (5) : find $\mathbf{u} \in \mathcal{U}$, $\forall \mathbf{v} \in \mathcal{V}$ such that

$$\int_{\Omega} \boldsymbol{\varepsilon}(\mathbf{u}) : \mathbf{C} : \boldsymbol{\varepsilon}(\mathbf{v}) d\Omega = \int_{\Omega} \mathbf{t} \cdot \mathbf{v} d\Gamma \quad \forall \mathbf{v}^h \in \mathcal{V}^h \tag{5}$$

where $\mathbf{u}$ is the trial function of the approximation and $\mathbf{v}$ is the test function. $\mathcal{U}$ and $\mathcal{V}$ are the trial and the test function spaces, respectively. The domain Ω is discretized into elements Ω^h and by following the standard Galerkin procedure, the continuous weak form is converted into a discrete weak form. The problem is to find $\mathbf{u} \in \mathcal{U}^h$, $\forall \mathbf{v} \in \mathcal{V}^h$ such that

$$a(\mathbf{u}^h, \mathbf{v}^h) = \ell(\mathbf{v}^h), \quad \forall \mathbf{v}^h \in \mathcal{V}^h \tag{6}$$

After substituting the piecewise approximation functions, we end up with a set of linear equations which are similar to the conventional FEM except for the integration procedure as follows:

$$\mathbf{K}\mathbf{u}^h = \mathbf{f} \tag{7}$$

where

$$\mathbf{K} = \int_{\Omega} \mathbf{B}^{\mathrm{T}}\mathbf{C}\mathbf{B}d\Omega \tag{8}$$

2.2 Strain smoothing

In SFEM, the integration is performed over smoothing domains rather the elements. In case of the ESFEM, the local smoothing domains are constructed based on the edges of elements. For a domain Ω with N number of edges, $\Omega = \Omega_e^1 \cup \Omega_e^2 \cup \cdots \Omega_e^N$ and $\Omega_e^i \cap \Omega_e^j = \varnothing$ for $i \neq j$. In the present study, triangular elements are considered and the smoothing domains are as shown in Fig. (1). For an edge k, the smoothing domain Ω_e^k is constructed by joining the nodes of the edges to the centroids of the adjacent elements. It can be seen in Fig. (1) that for some edges, the smoothing domains are triangular and contribute to only one element while others are quadrilateral and contribute to two elements. However, the shape functions remain the same as the parent element. At a point $\mathbf{x}$ in domain Ω^k, the smoothed derivative of the shape function, $N_I(\mathbf{x})$, is given by

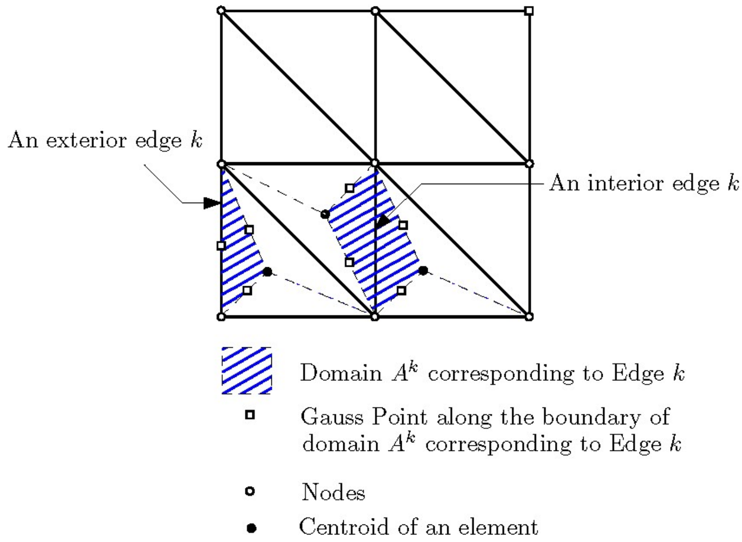

Fig. 1. Schematic illustration of the construction of smoothing cell in the ESFEM. The smoothing cell is constructed by connecting the centers of the elements that make up an edge with the element vertices. The shaded region is the smoothing cell.

$$\tilde{N}_{I,i}(\mathbf{x}) = \int_{\Omega^k} N_{I,i}(\mathbf{x})\Phi(\mathbf{x})d\Omega \tag{9}$$

where $\Phi(\mathbf{x})$ is the smoothing function and $i = x, y$. In this case, we use a piecewise constant function defined as follows:

$$\Phi(\mathbf{x}) = \begin{cases} \dfrac{1}{A_e^k}, & \mathbf{x} \in \Omega_e^k \\ 0, & \mathbf{x} \notin \Omega_e^k \end{cases} \tag{10}$$

where A_e^k is the area of the smoothing domain Ω_e^k corresponding to edge k, given by:

$$A_e^k = \int_{\Omega_e^k} d\Omega = \frac{1}{3}\sum_{J=1}^{N_e^k} A^J \tag{11}$$

where N_e^k represents the number of elements around the edge k and A^J is the area of the J^{th} element adjacent to the edge k. As noted earlier, irrespective of the element, $N_e^k = 1$ for an edge along the domain boundary and $N_e^k = 2$ for all other inner edges. Once all the derivatives are found, the smoothed strain displacement matrix is assembled as in the regular FEM by replacing the compatible strain operators with the smoothed strain operators. For any polygon, the smoothed strain displacement matrix corresponding to the support domain based on the ESFEM is given by

$$\tilde{\mathbf{B}}(\mathbf{x}) = \left[\tilde{\mathbf{B}}_1(\mathbf{x}), \tilde{\mathbf{B}}_2(\mathbf{x}), \cdots, \tilde{\mathbf{B}}_n(\mathbf{x})\right] \tag{12}$$

where,

$$\tilde{\mathbf{B}}_I(\mathbf{x}) = \begin{bmatrix} \tilde{N}_{I,x}(\mathbf{x}) & 0 \\ 0 & \tilde{N}_{I,y}(\mathbf{x}) \\ \tilde{N}_{I,y}(\mathbf{x}) & \tilde{N}_{I,x}(\mathbf{x}) \end{bmatrix} \quad \text{where,} \quad I = 1, 2, \cdots, n \tag{13}$$

where, n is the number of nodes that contribute to the domain Ω_e^k, n =3 for boundary edges, and n = 4 for interior edges. However, it should be noted that the above-mentioned expression is evaluated by applying the Divergence theorem to Eq. (9) as shown below:

$$\tilde{N}_{I,i}(\mathbf{x}) = \frac{1}{A_e^k} \int_{\Gamma^k} N_I(\mathbf{x}) \mathbf{n}^s(\mathbf{x}) d\Gamma \tag{14}$$

where, $\mathbf{n}^s$ is the normal to the segment $\Gamma_s^k \in \Gamma^k$ of the boundary corresponding to edge k given by

$$\mathbf{n}^s(\mathbf{x}) = \begin{bmatrix} n_x^s(\mathbf{x}) & 0 \\ 0 & n_y^s(\mathbf{x}) \\ n_y^s(\mathbf{x}) & n_x^s(\mathbf{x}) \end{bmatrix} \tag{15}$$

2.3 Stiffness matrix formulation

The smoothed derivative in the domain corresponding to edge k is numerically computed as

$$\tilde{N}_{I,i}(\mathbf{x}) = \frac{1}{A_e^k} \sum_{s=1}^{N_s} \sum_{g=1}^{G_k} N_I(\mathbf{x}_g) n_i^s(\mathbf{x}_g) l_s^k \quad \text{where,} \quad i = x, y \tag{16}$$

where, A_e^k is the area of the smoothing domain Ω_e^k, N_s is the number of segments along the boundary Γ^k of the domain Ω_e^k, and G_k is the number of Gauβ points along the segment Γ_s^k. l_s^k and n_i^s are the length and unit outward normal of segment Γ_s^k respectively. The smoothed stiffness matrix is then given by:

$$\tilde{\mathbf{K}} = \sum_{k=1}^{N} \tilde{\mathbf{K}}_k = \sum_{k=1}^{N} \int_{\Omega_e^k} \tilde{\mathbf{B}}^{\mathrm{T}} \mathbf{C} \tilde{\mathbf{B}} \mathrm{d}\Omega = \tilde{\mathbf{B}}^{\mathrm{T}} \mathbf{C} \tilde{\mathbf{B}} A_e^k \tag{17}$$

where $\tilde{\mathbf{K}}_k$ represents the smoothed stiffness matrix computed over the smoothing domain associated with edge k.

Note: The smoothed strain can also be computed directly from the compatible strains by averaging it in the domain. However, it require derivatives and Jacobian to be evaluated unlike the aforementioned method.

3. SBFEM formulation

The scaled boundary polygon is used to capture the singular fields at the vicinity of the crack -tip as shown in Fig. (2). The crux of the SBFEM lies in scaling the polygon with respect to the scaling center with a dimensionless parameter ξ which has a value of 0 at the scaling center and a value of 1 on the boundary as shown in Fig. (2). The scaling center has to satisfy the scaling requirement, therefore, it is chosen inside the scaled boundary polygon such that the whole boundary is visible. The boundary of the polygon is defined in terms of circumferential coordinate η discretized by using the finite element shape functions. Important equations to obtain the stiffness matrix and the SIFs using the SBFEM are summarized in this section.

3.1. Stiffness matrix from the SBFEM

The transformation of the Cartesian coordinate system to the scaled boundary coordinates is related as

$$\mathbf{x} = \xi x(\eta) = \xi \mathbf{N}(\eta) \mathbf{x} \tag{18}$$

where $\mathbf{x}$ is a point in the domain and $\mathbf{N}(\eta)$ is the shape function defined as

$$\mathbf{N}(\eta) = [N_1(\eta)\mathbf{I}, N_2(\eta)\mathbf{I}, \cdots, N_M(\eta)\mathbf{I}] \tag{19}$$

M is the number of nodes of an edge of a scaled boundary polygon and $\mathbf{I}$ is the identity matrix of size 2×2. The displacement field at a point inside the domain in the scaled boundary coordinates is obtained by interpolating $\mathbf{u}(\xi)$ with shape functions on the boundary of the polygon in circumferential direction as

$$\mathbf{u}(\xi,\eta) = \mathbf{N}(\eta)\mathbf{u}(\xi) \tag{20}$$

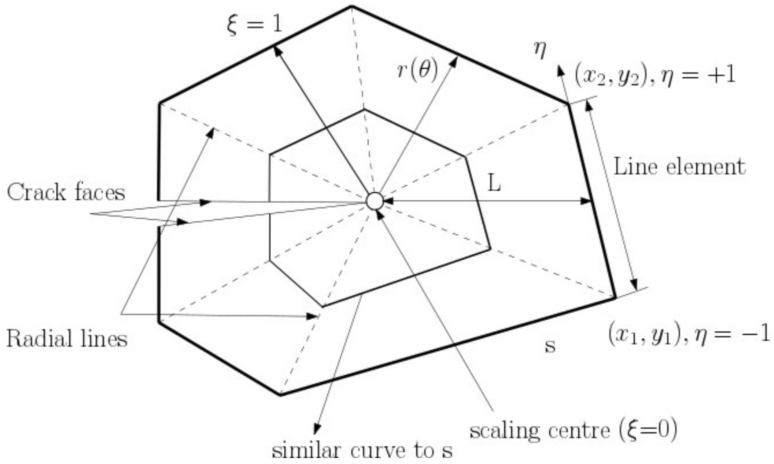

Fig. 2. Illustration of the scaled boundary coordinate system for a cracked domain. The scaling center is chosen at the crack tip.

The strain field in the scaled boundary coordinates is obtained by substituting Eq. (20) into Eq. (3) which is written as

$$\boldsymbol{\varepsilon}(\xi,\eta) = \mathbf{B}_1(\eta)\mathbf{u}(\xi)_{,\xi} + \frac{1}{\xi}\mathbf{B}_2(\eta)\mathbf{u}(\xi) \tag{21}$$

The stress field in the scaled boundary coordinates is obtained by substituting Eq. (21) into Eq. (4) as

$$\boldsymbol{\sigma}(\xi,\eta) = \mathbf{C}\left(\mathbf{B}_1(\eta)\mathbf{u}(\xi)_{,\xi} + \frac{1}{\xi}\mathbf{B}_2(\eta)\mathbf{u}(\xi) \right) \tag{22}$$

where $\mathbf{B}_1$ and $\mathbf{B}_2$ are the strain displacement matrices as mentioned in [25]. The stress and strain fields obtained are substituted in virtual work equation and by invoking the arbitrariness of the displacement in the radial direction, the scaled boundary finite element equation in the displacement is obtained as

$$\mathbf{E}_0\xi^2\mathbf{u}(\xi)_{,\xi\xi} + (\mathbf{E}_0 - \mathbf{E}_1 + \mathbf{E}_1^{\mathrm{T}})\xi\mathbf{u}(\xi)_{,\xi} - \mathbf{E}_2\mathbf{u}(\xi) = \mathbf{0} \tag{23}$$

which describes the equilibrium in the radial direction with $\mathbf{q}(\xi)$ as the internal nodal forces on a surface with a constant ξ.

$$\mathbf{q}(\xi) = \mathbf{E}_0\xi\mathbf{u}(\xi)_{,\xi} + \mathbf{E}_1^{\mathrm{T}}\mathbf{u}(\xi) \tag{24}$$

$\mathbf{E}_0$, $\mathbf{E}_1$, and $\mathbf{E}_2$ are the coefficient matrices that are related to the boundary and the material properties of the domain as defined in [25]. It should be noted that Eq. (23) is a homogeneous second-order differential equation with displacements as unknowns. It can be transformed into a system of first-order ODEs using

$$\xi \begin{Bmatrix} \mathbf{u}(\xi) \\ \mathbf{q}(\xi) \end{Bmatrix}_{,\xi} = \mathbf{Z} \begin{Bmatrix} \mathbf{u}(\xi) \\ \mathbf{q}(\xi) \end{Bmatrix} \tag{25}$$

where $\mathbf{Z}$ is the Hamiltonian matrix.

$$\mathbf{Z} = \begin{bmatrix} \mathbf{E}_0^{-1}\mathbf{E}_1^{\mathrm{T}} & -\mathbf{E}_0^{-1} \\ -\mathbf{E}_2 + \mathbf{E}_1\mathbf{E}_0^{-1}\mathbf{E}_1^{\mathrm{T}} & -\mathbf{E}_1\mathbf{E}_0^{-1} \end{bmatrix} \tag{26}$$

The transformation leading to real Schur form matrix $\mathbf{S}$, is expressed as

$$\mathbf{Z}\begin{bmatrix} \boldsymbol{\psi}_u \\ \boldsymbol{\psi}_q \end{bmatrix} = \begin{bmatrix} \boldsymbol{\psi}_u \\ \boldsymbol{\psi}_q \end{bmatrix}\mathbf{S} \tag{27}$$

For a bounded domain, the values corresponding to the negative eigenvalues of $\mathbf{Z}$ gives finite displacements at the scaling center. Therefore, the solution to Eq. (25) is

$$\mathbf{u}(\xi) = \boldsymbol{\psi}_u\xi^{-\mathbf{s}}\mathbf{c} \tag{28}$$

$$\mathbf{q}(\xi) = \boldsymbol{\psi}_q\xi^{-\mathbf{s}}\mathbf{c} \tag{29}$$

Here, Eqs. (28) and (29) are calculated around the boundary of the polygon $(\xi = 1)$ and eliminating the term **c** leads to

$$\mathbf{q} = \boldsymbol{\psi}_q \boldsymbol{\psi}_u^{-1} \mathbf{u} \tag{30}$$

The static stiffness matrix of the scaled boundary polygon is

$$\mathbf{K}^{\mathrm{SBFEM}} = \boldsymbol{\psi}_q \boldsymbol{\psi}_u^{-1} \tag{31}$$

The integration constants $\mathbf{c}$ are determined by the nodal displacements on the boundary $\mathbf{u}_b = \mathbf{u}(\xi = 1)$. Substituting $\xi = 1$ into Eq. (28) leads to

$$\mathbf{c} = \boldsymbol{\psi}_u^{-1} \mathbf{u}_b \tag{32}$$

3.2. SIFs using the SBFEM

The stress at a point in the scaled boundary coordinate is obtained by substituting Eq. (28) into Eq. (22).

$$\boldsymbol{\sigma} = \boldsymbol{\Psi}_\sigma \xi^{-\mathbf{S}-\mathbf{I}} \mathbf{c} \tag{33}$$

where $\mathbf{I}$ is the identity matrix and $\boldsymbol{\Psi}_\sigma$ are the stress modes corresponding to the displacement modes $\boldsymbol{\Psi}_u$ defined as

$$\boldsymbol{\Psi}_\sigma = \mathbf{c}\left(\mathbf{B}_1(\eta)\boldsymbol{\psi}_u \mathbf{S} + \mathbf{B}_2(\eta)\boldsymbol{\psi}_u\right) \tag{34}$$

At the crack tip, the stress modes corresponding to the singularity contributes and all other modes vanishes as $\xi \to 0$. The stresses corresponding to the singular stress mode is written as

$$\boldsymbol{\sigma}^{(s)} = \boldsymbol{\Psi}_\sigma^{(s)} \xi^{-\mathbf{S}^{(s)}-\mathbf{I}} \mathbf{c}^{(s)} \tag{35}$$

The superscript (s) refers to the stress modes corresponding to the singular fields at the crack tip. For an elastic, isotropic, and homogeneous material, the matrix $\mathbf{S}^{(s)}$ is a 2×2 diagonal matrix with the strength of singularities of crack-tip sitting along the diagonal of the matrix. The SIFs $\mathbf{K}(\theta) = \left[K_I(\theta), K_{II}(\theta)\right]^{\mathrm{T}}$ are written in terms of the scaled boundary coordinates as

$$\mathbf{K}(\theta) = \sqrt{2\pi L}\, \boldsymbol{\Psi}_\sigma^{(s)} \left(\frac{L}{r(\theta)}\right)^{-\mathbf{S}^{(s)}-\mathbf{I}} \mathbf{c}^{(s)} \tag{36}$$

where L is the characteristic length and $r(\theta)$ is the radial distance at an angle θ from the crack tip to the boundary as shown in Fig. (2).

4. Coupling of the ESFEM and the SBFEM

Since the effect of singularity is limited only to a small region around the crack tip, it is sufficient to treat this small region via the SBFEM. In the present study, triangular meshes are used since they can be easily generated even for complex structures. Since the regular FEM requires the computation of derivatives and also imposes mesh quality conditions such as in the internal angles of the elements, meshing becomes non-trivial even with triangular elements. Moreover, triangular meshes are also less accurate due to the low order of approximation of the field. Therefore, SFEM is used in this study along with in particular the ESFEM, which has been shown to be more accurate than the other versions, sometimes even outperforming 4-noded linear elements. Therefore, the ESFEM is used for the remaining portion of the domain. Since we deal with linear problems, the stiffness matrix of the domain is independent of the solution and can be found separately. The stiffness matrix of the SBFEM domain is computed based on the linear boundary elements and the ESFEM is used elsewhere. The stiffness matrix obtained from both methods are assembled as in conventional finite elements and solved for unknown displacements and stresses. It can be seen in Fig. (3) that the support domain for the edges along the SBFEM domain boundary partly overlap with the SBFEM domain. Therefore, much care is needed in evaluating the gradients in the ESFEM. Only the domain shown in Fig. (3(b)) should be considered contributing to the stiffness matrix computed via the ESFEM. The stiffness matrices are then assembled as per corresponding degrees of freedom indices and solved for the unknown displacements. The nodal displacements are used as the input for computing the strength of singularity and the SIFs via the SBFEM. To evaluate the SIFs, the stress modes corresponding to the scaled boundary domain are calculated using Eq. (35) and the SIFs from the Eq. (36).

5. Numerical section

In this section, the robustness of the proposed formulation is demonstrated along with a few standard benchmark examples from the linear elastic fracture mechanics. The influence of mesh size and the size of the scaled boundary domain on the stress intensity factors are studied. The results from the present simulation, especially the mode-I and mode-II stress intensity factors are compared with empirical solutions. Unless mentioned otherwise, the following material properties are chosen: Young's modulus of $E = 3\times 10^7\,\mathrm{Pa}$ and Poisson's ratio of $\nu = 0.3$. For all the examples, a state of plane strain condition is assumed.

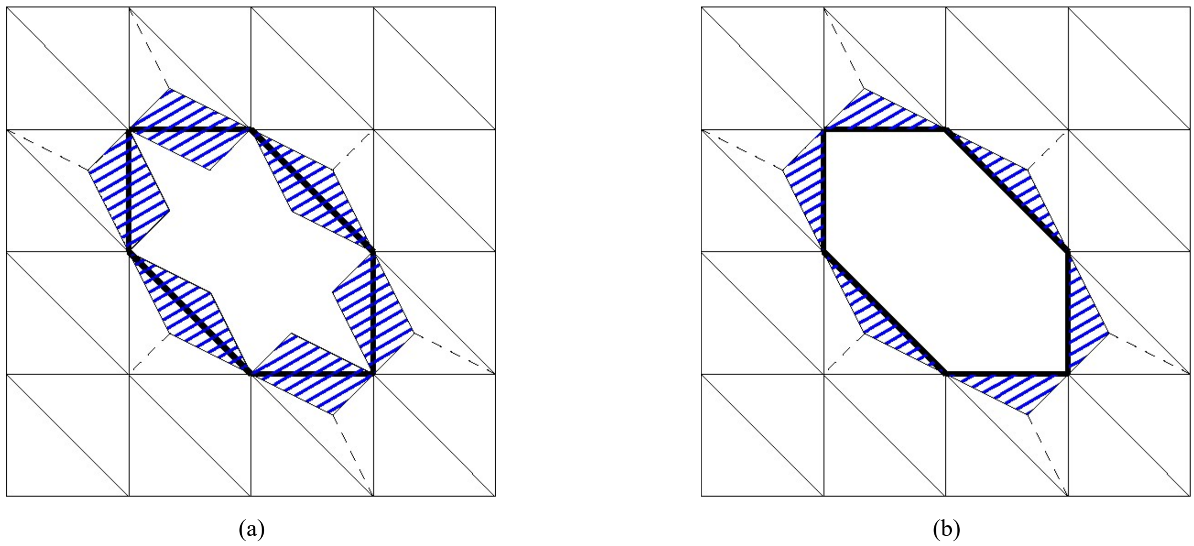

Fig. 3. Smoothing domain based on the ESFEM corresponding to the bold edges along the boundary of SBFEM domain (a) Default domain when the ESFEM is used all through (b) Actual domain considered in the current case.

5.1 Edge crack under pure mode-I

In this first example, a plate with an edge crack under uniform tension of $\sigma = 1.0\,\text{Pa}$ as shown in Fig. (4), is considered. The dimensions of the plate are 1mm × 2mm with crack length of $a = 0.5\text{mm}$. The empirical solution for the mode-I SIF, K_I is given by

$$K_I^{\text{REF}} = c\sigma\sqrt{\pi a} = 3.5423\text{Pa}\sqrt{mm} \tag{37}$$

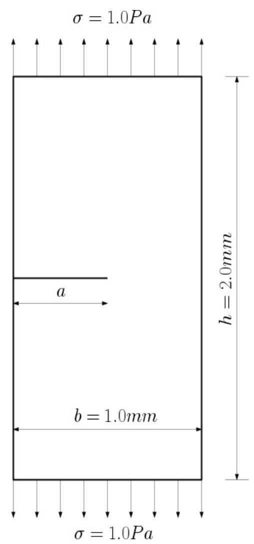

Fig. 4. Details of a finite plate with an edge crack under tensile stresses

where $c = 1.12 - 0.231\left(\frac{a}{b}\right) + 10.55\left(\frac{a}{b}\right)^2 - 21.72\left(\frac{a}{b}\right)^3 + 30.39\left(\frac{a}{b}\right)^4$ is the finite geometry correction factor. The domain is discretized with 3-noded triangular elements. In this study, a sample mesh employed as shown in Fig. (5). A region in the vicinity of the crack tip is identified and is replaced with the scaled boundary region. The choice of the shape of the scaled boundary region is arbitrary. In this example, the scaled boundary region is identified by performing a search algorithm of elements that are associated with the element containing the crack tip. This results in a `hexagon' shaped region (Fig. 5).

The red line in Fig. (5) represents the crack. The stiffness matrices of the constant strain triangular elements are obtained by using the ESFEM and the hexagonal region is treated as the scaled boundary polygon with linear elements around the boundary. The crack tip is taken to be the center of the scaled boundary region. The salient feature, as mentioned before, is that singularity of any order can be represented semi-analytically. However, the accuracy of it depends on the discretization employed on the boundary of the scaled boundary element. In this case, it is associated with the underlying triangular mesh. Once the scaled boundary region is identified, the degrees of freedom of internal nodes are condensed during the solution process. The number of elements on the boundary can be increased by maximizing the size of the scaled boundary domain.

A study on the convergence of the strength of singularity and mode I SIF of the crack is carried out by increasing the number of line elements around the scaled boundary polygon with a constant mesh consisting of 3321 nodes (6400 elements). The results are presented in Table (1). It can be observed that the strength of singularity converges to the theoretical value of 0.5 as the number of line elements around the boundary of the scaled boundary polygon is increased. Table (1) shows that the stress intensity factors converge to the empirical solution as the number of sides of the scaled boundary polygon are increased.

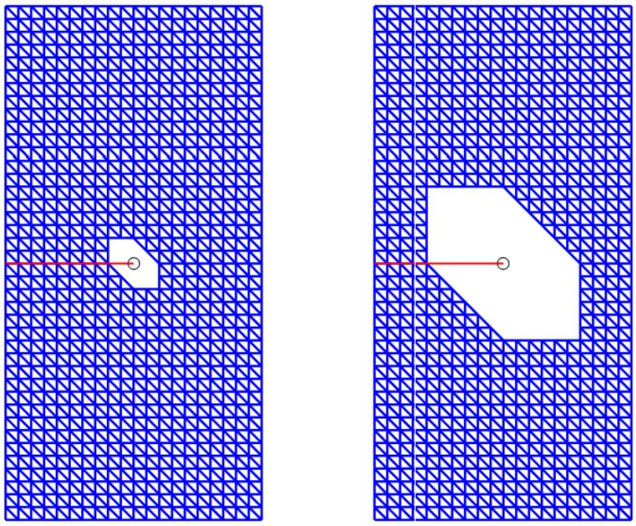

Fig. 5. A fixed mesh (mesh: 21x41 nodes) for two cases of scaled boundary domains (red color line represents initial crack length; black color circle represents the scaling center): a) 12 linear elements along the boundary of the scaled boundary polygon. b) 36 linear elements along the boundary of the scaled boundary polygon.

Table 1. Convergence of the strength of singularity for a domain with an edge crack with number of elements around the scaled boundary region. The domain is discretized with T3 elements consisting of 3321 nodes (6400 elements). The crack length is taken as a = 0.5mm.

Number of elements	6	12	24	48	96
S11	0.5031	0.5182	0.5036	0.5009	0.5002
S22	0.5031	0.4925	0.4991	0.4998	0.4999
KI	4.6121	4.1400	3.7585	3.36399	3.5875

As can be seen, Fig. (6) shows the convergence of the SIF with increasing number of degrees of freedom. Three different crack lengths are studied. Though the SIF increases with the crack length, it is observed that the value of SIFs have similar convergence for different crack lengths. Therefore, it can be inferred that the accuracy and the rate of convergence of K_I depends on the number of elements in the scaled boundary polygon while it is independent of the crack length.

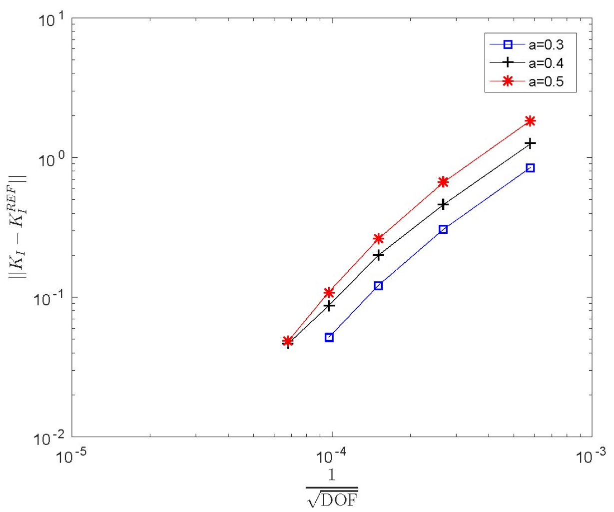

Fig. 6. Convergence of the SIF for an edge crack domain under mode I for different crack lengths.

A crack propagation study is carried out for the same problem. The domain is discretized using 3321 nodes. Based on the previous studies, a SBFEM domain consisting of 48 linear elements is used around the crack tip. The maximum circumferential stress criterion [26] is used to predict the crack propagation angle (c.f Eq. (38)). This criterion is based on the assumption that the crack propagates in the direction normal to the maximum circumferential stress.

$$\theta_c = 2arctan\left(\frac{K_I - \sqrt{K_I^2 + 8K_{II}^2}}{4K_{II}}\right) \tag{38}$$

The values of K_I , K_{II} , and θ of the crack during different stages of the crack growth are presented in Table (2). The small deviation in the crack path is adjusted locally in the scaled boundary domain retaining the existing ESFEM mesh without any changes. Different stages of the crack growth are shown in Fig. (7).

Table 2. SIFs and angle of inclination at various stages of the crack growth

Crack width	KI	KII	θ
0.3	1.7125	2.59 x 10-3	-3.03 x 10-3
0.4	2.1779	2.82 x 10-3	-2.59 x 10-3
0.5	2.9123	3.96 x 10-3	-2.72 x 10-3
0.6	4.1556	0.0062	-0.00299
0.7	6.5423	0.0102	-0.00314

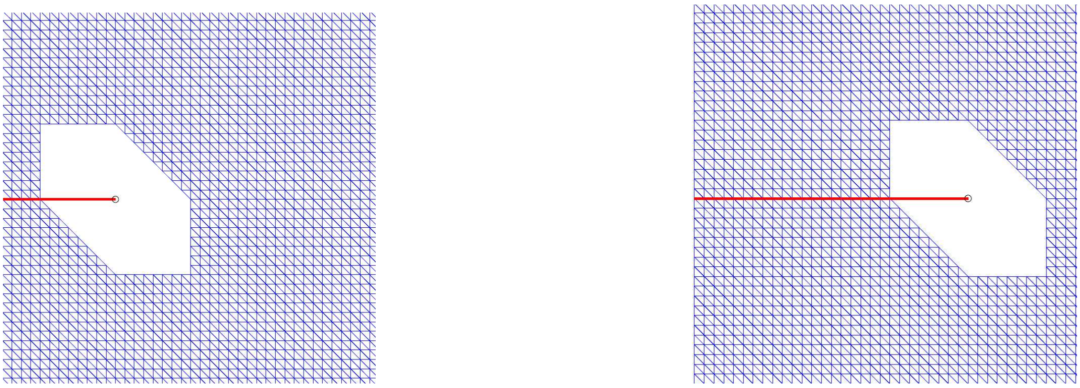

(a) Crack width=0.3 units (b) Crack width=0.7 units

Fig. 7. Crack trajectory in a plate with an edge crack under tensile loading at different stages of growth with increments of 0.1 units. The black circle shows the scaling center. The SBFEM domain is shifted as the crack propagates.

5.2. Edge crack under mixed mode

In this stage, a plate with an edge crack under mixed mode loading condition is chosen. The geometry and the loading conditions of the domain are as shown in Fig. (8). The dimensions of the plate are 7mm × 16mm with a crack length of $a = 3.5\text{mm}$. The reference solution for an edge crack problem under shear load is

$$K_I = 34.0\text{Pa}\sqrt{\text{mm}}, \quad K_{II} = 4.55\text{Pa}\sqrt{\text{mm}} \tag{39}$$

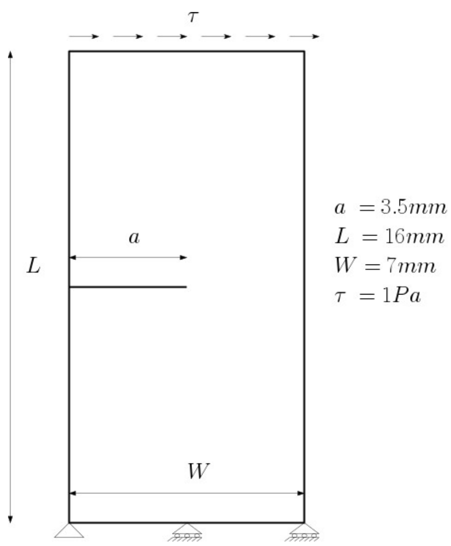

Fig. 8. Mixed mode: Geometry and boundary conditions

The convergence of the SIFs K_I and K_{II} are studied with increasing number of degrees of freedom. Based on the results in the previous numerical example (Table (1)), a minimum of 48 linear elements are used along the boundary of the scaled boundary polygon to better capture the singularity at the vicinity of the crack-tip. Finite element meshes, as shown in Fig. (5), are adopted. It can be seen in Fig. (9) that the SIF converges to the reference solution with increasing number of nodes.

The crack propagation for the same problem is simulated with the proposed technique. The domain with an edge crack is discretized as shown in Fig. (10a). In the vicinity of the crack tip, a square domain is identified from the base mesh. The continuous red line in Fig. (10a) represents the initial crack and to simulate the crack faces, the nodes along the red line are duplicated. The stiffness matrices of the T3 elements are computed by using the ESFEM and the stiffness matrix of the square domain is computed by using the SBFEM. On the other hand, Fig. (10b) is the zoomed view of the scaled boundary polygon as in Fig. (10a) with the scaling center located at the crack tip represented by the black circle. The maximum circumferential stress criterion is used to predict the crack propagation angle. The crack incremental length is chosen as Δa = 0.5. After the crack kinks, the domain is discretized again and a square SBFEM domain is identified from the new mesh such that it aligns to the crack tip as shown in Fig. (11a) with the scaling center (black circle) at the crack tip. The length of the SBFEM domain is taken as twice the length of the crack incremental length and the scaling center is chosen at the crack-tip. Moreover, Figs. (11a) and (11b) depicts the discretization of the domain at the 2nd and the 4th incremental step. The red line in Fig. (11) represents the predicted crack path. To obtain the crack path, the scaling center corresponding to each incremental step of the SBFEM domain is chosen and plotted. On the other hand, Fig. (12) shows the crack path obtained from the proposed technique with 7 incremental steps choosing Δa = 0.5. It is observed that the crack path from the present technique is consistent with that reported in [27].

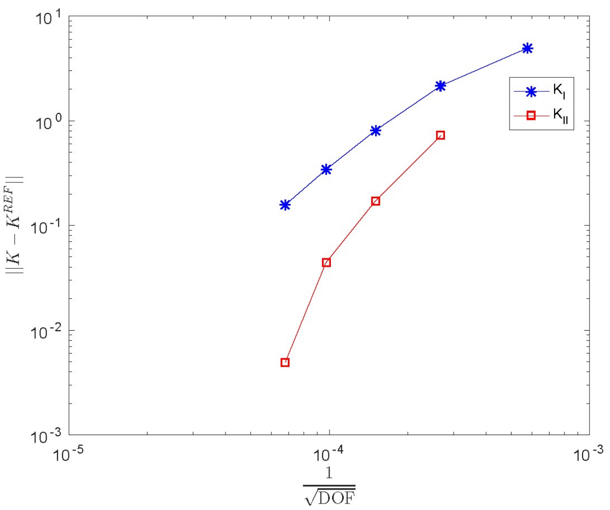

Fig. 9. Convergence of the SIF for an edge crack domain under shear stress

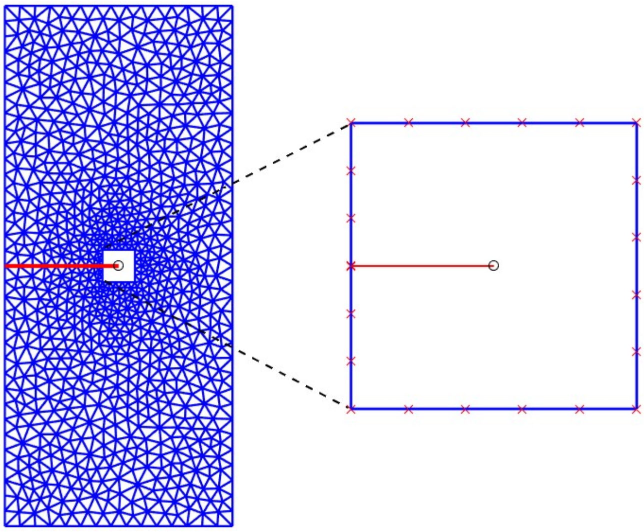

Fig. 10. (a) Discretization of an edge crack plate under mixed mode (black circle represents the scaling center and the red line represents the initial crack length), (b) Zoomed view of the SBFEM domain (red color 'x' represents nodes around the boundary of the scaled boundary polygon). For color illustration, readers are referred to the online version.

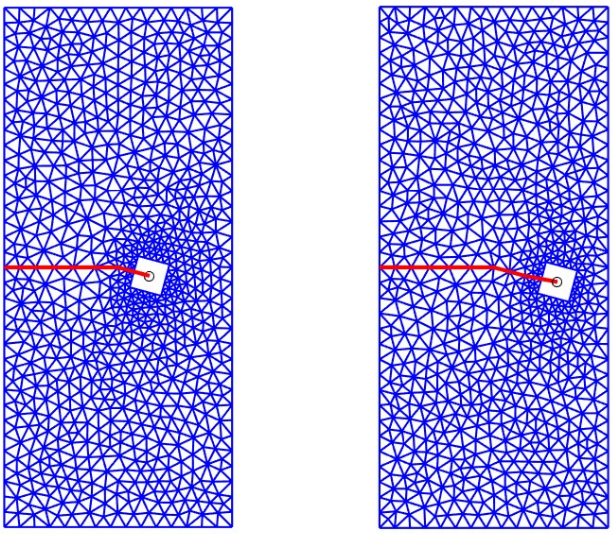

Fig. 11. Discretization of an edge crack plate under mixed mode: (a) 2nd incremental step and (b) 4th incremental step (red line represents the predicted crack path).

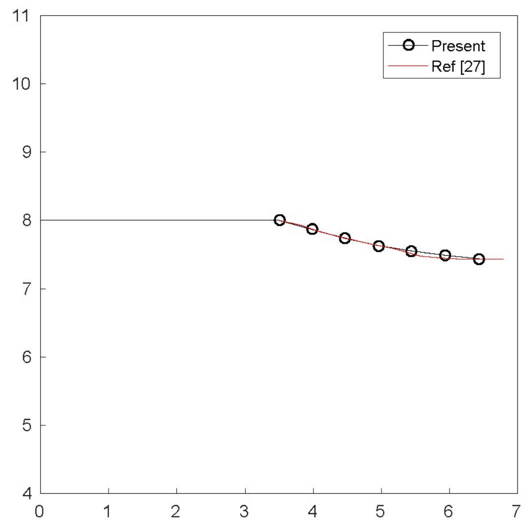

Fig. 12. Crack path of a plate with an edge crack under mixed mode loading with a crack increment of Δa = 0.5.

6. Conclusion

A technique to evaluate fracture parameters combining the ESFEM and the SBFEM is presented. The ESFEM is used to calculate the stiffness matrix of the domain away from the crack tip and the SBFEM is used to calculate the stiffness matrix of the domain at the vicinity of the crack tip in order to capture the crack-tip singularity. The size of the SBFEM domain depends on the accuracy with which the strength of singularity needs to be represented. The presented technique doesn't require any prior knowledge of asymptotic behavior near crack-tip fields. Numerical results show the accuracy and the efficiency of the proposed technique. The computed SIFs are in good agreement with the reference solutions. Crack propagation is also carried out to study the versatility of the proposed method. The predicted crack trajectories agree well with the references. Moreover, it is noted that only minimal re-meshing is required locally around the crack tip. The important conclusions in coupling the ESFEM and the SBFEM are as follows:

- The convergence of the stress intensity factor is independent of the crack length.
- For a fixed number of elements in the scaled boundary polygon, singularity is independent of the global mesh.
- For a fixed global mesh size, the strength of singularity is independent of the crack size and improves with increasing number of degrees of freedom of the scaled boundary polygon.

Conflict of Interest

The author(s) declared no potential conflicts of interest with respect to the research, authorship and publication of this article.

Funding

The author(s) received no financial support for the research, authorship and publication of this article.

References

[1] Song, J.H., Areias, P.M.A., Belytschko, T., A method for dynamic crack and shear band propagation with phantom nodes. *International Journal for Numerical Methods in Engineering*, 67(6), 2006, 868–893.

[2] Hamdia, K.M., Silani, M., Zhuang, X., He, P., Rabczuk, T., Stochastic analysis of the fracture toughness of polymeric nanoparticle composites using polynomial chaos expansions. *International Journal of Fracture*, 206(2), 2017, 215–227.

[3] Braun, J., Sambridge, M., A numerical method for solving partial differential equations on highly irregular evolving grids. *Nature*, 376, 1995, 655–660.

[4] Hughes, T.J.R., Cottrell, J.A., Bazilevs, Y., Isogeometric analysis: Cad, finite elements, nurbs, exact geometry and mesh refinement. *Computer Methods in Applied Mechanics and Engineering*, 194(39), 2005, 4135 – 4195.

[5] Ghorashi, S.Sh., Valizadeh, N., Mohammadi, S., Rabczuk, T., T-spline based xiga for fracture analysis of orthotropic media. *Computers and Structures*, 147, 2015, 138 – 146, CIVIL-COMP.

[6] Valizadeh, N., Bazilevs, Y., Chen, J.S., Rabczuk, T., A coupled igameshfree discretization of arbitrary order of accuracy and without global geometry parameterization. *Computer Methods in Applied Mechanics and Engineering*, 293, 2015, 20 – 37.

[7] Liu, G.R., Dai, K.Y., Nguyen, T.T., A smoothed finite element method for mechanics problems. *Computational Mechanics*, 39(6), 2007, 859–877.

[8] Bordas, S.P.A., Rabczuk, T., Hung, N.X., Nguyen, V.P., Natarajan, S., Bog, T., Quan, D.M., Hiep, N.V., Strain smoothing in fem and xfem. *Computers & structures*, 88(23), 2010, 1419–1443.

[9] Surendran, M., Natarajan, S., Bordas, S.P.A., Palani, G.S., Linear smoothed extended finite element method. *International Journal for Numerical Methods in Engineering*, 112(12), 2017, 1733–1749.

[10] Nguyen-Thoi, T., Liu, G.R., Nguyen-Xuan, H., An n-sided polygonal edge-based smoothed finite element method (nes-fem) for solid mechanics. *International Journal for Numerical Methods in Biomedical Engineering*, 27(9), 2011, 1446–1472.

[11] Dai, K.Y., Liu, G.R., Nguyen, T.T., An n-sided polygonal smoothed finite element method (nsfem) for solid mechanics. *Finite Elements in Analysis and Design*, 43(11), 2007, 847 – 860.

[12] Francis, A., Ortiz-Bernardin, A., Bordas, S.P.A., Natarajan, S., Linear smoothed polygonal and polyhedral finite elements. *International Journal for Numerical Methods in Engineering*, 109(9), 2017, 1263–1288.

[13] Liu, G.R., Nguyen-Thoi, T., Lam, K.Y., An edge-based smoothed finite element method (es-fem) for static, free and forced vibration analyses of solids. *Journal of Sound and Vibration*, 320(4), 2009, 1100–1130.

[14] Song, C., Wolf. J.P., Consistent infinitesimal finite-element cell method: three-dimensional vector wave equation. *International Journal for Numerical Methods in Engineering*, 39, 1996, 2189–2208.

[15] Song, C., Wolf, J.P., The scaled boundary finite-element methodalias consistent infinitesimal finite-element cell methodfor elastodynamics. *Computer Methods in Applied Mechanics and Engineering*, 147(3-4), 1997, 329–355.

[16] Ooi, E.T., Natarajan, S., Song, C., Ooi, E.H., Dynamic fracture simulations using the scaled boundary finite element method on hybrid polygon-quadtree meshes. *International Journal of Impact Engineering*, 90, 2016, 154–164.

[17] Song, C., Tin-Loi, F., Gao, W., A definition and evaluation procedure of generalized stress intensity factors at cracks and multi-material wedges. *Engineering Fracture Mechanics*, 77(12), 2010, 2316–2336.

[18] Natarajan, S., Song, C., Representation of singular fields without asymptotic enrichment in the extended finite element method. *International Journal for Numerical Methods in Engineering*, 96(13), 2013, 813–841.

[19] Li, C., Man, H., Song, C., Gao, W., Fracture analysis of piezoelectric materials using the scaled boundary finite element method. *Engineering Fracture Mechanics*, 97(1), 2012, 52–71.
[20] Tat, E., Sundararajan, O., Song, C., Tin-loi, F., Crack propagation modelling in functionally graded. 2015, p.p. 87–105.
[21] Ooi, E.T., Song, C., Tin-Loi, F., A scaled boundary polygon formulation for elasto-plastic analyses. *Computer Methods in Applied Mechanics and Engineering*, 268, 2014, 905–937.
[22] Song, C., Wolf, J.P., Semi-analytical representation of stress singularities as occurring in cracks in anisotropic multi-materials with the scaled boundary finite-element method. *Computers and Structures*, 80(2), 2002, 183–197.
[23] Chen, J.S., Wu, C.T., Yoon, S., You, Y., A stabilized conforming nodal integration for galerkin mesh-free methods. *International journal for numerical methods in engineering*, 50(2), 2001, 435–466.
[24] Liu, G.R., Nguyen-Thoi, T., Nguyen-Xuan, H.B., Lam, K.Y., A node-based smoothed finite element method (ns-fem) for upper bound solutions to solid mechanics problems. *Computers & structures*, 87(1), 2009, 14–26.
[25] Deeks, A.J., Wolf, J.P., A virtual work derivation of the scaled boundary finite-element method for elastostatics. *Computational Mechanics*, 28(6), 2002, 489–504.
[26] Sih, G.C., Strain-energy-density factor applied to mixed mode crack problems, *International Journal of Fracture*, 10(3), 1974, 305–321.
[27] Rao, B.N., Rahman, S., A coupled meshless-finite element method for fracture analysis of cracks. *International Journal of Pressure Vessels and Piping*, 78, 2001, 647 –657.